

Hybrid 3D Dynamic Measurement by Particle Swarm Optimization and Photogrammetric Tracking

M. Shahbazi

Centre d'applications et de recherches en télédétection and department of applied geomatics, Université de Sherbrooke, Boul. de l'Université, 2500, J1K 2R1, Sherbrooke, Quebec, Canada, mozhdeh.shahbazi@usherbrooke.ca

High-accuracy motion modeling in three dimensions via digital images has been increasingly the matter of interest in photogrammetry and computer vision communities. Although accurate sub-pixel image registration techniques are the key elements of measurement, they still demand enhanced intelligence, autonomy, and robustness. In this paper, a new correlation-based technique of stereovision is proposed to perform inter-frame feature tracking, inter-camera image registration, and to measure the 3D state vector of features simultaneously. The developed algorithm is founded on population-based intelligence (particle swarm optimization) and photogrammetric modeling. The proposed technique is mainly aimed at reducing the computational complexities of non-linear optimization methods of digital image registration for deformation measurement, and passing through 2D image correlation to 3D motion modeling. The preliminary results have illustrated the feasibility of this technique to detect and measure sub-millimeter deformations by performing accurate, sub-pixel image registration.

Keywords: Swarm intelligence, photogrammetry, registration, calibration, 3D measurement.

1. INTRODUCTION

OPTICAL METHODS for 3D deformation measurement are emerging significantly in various fields of science, military services, and entertainment industry, e.g., mechanical, material, and structural engineering, remote sensing and telemetry, reconnaissance and surveillance, as well as animation generation. These methods are mainly divided into two categories: interferometric and non-interferometric optical techniques.

Interferometric techniques measure the displacements by fringe projection and phase-shifting methods. Therefore, a source of light projection is required, which makes these techniques more cumbersome regarding the experimental conditions. Non-interferometric techniques use the gray-level variations of images to detect the deformations. The principal process of such workflows is to match, namely to track, the same objects in multiple images, whether on frame sequences and/or stereo views. While applying digital image correlation (DIC) on frame sequences of a single camera results in limited in-plane movements, stereovision techniques provide a facility for three-dimensional change measurement.

Many studies have been dedicated to these fields, a review of which can be found in the literature [1], [2]. As the most general and popular matching practice, a matching objective function, such as a zero-mean normalized cross-correlation (ZNCC), is optimized on image subsets by different algorithms like iterative Newton–Raphson (NR) algorithm or least squares (LS) adjustment. A sub-pixel interpolation algorithm, such as bilinear or bicubic interpolation scheme, should also be considered for determining the intensity and gradient values.

As non-linear optimization techniques, NR, LS and similar algorithms require initial approximation with accuracy of a few pixels to converge rapidly and correctly [3]–[5]. The conventional technique for estimating the initial position of a corresponding feature is to perform an exhaustive coarse-

matching by displacing the matching kernel by integer increments over a predefined area. Several techniques are proposed to improve the initial guess, for example by image rectification [6], by reliability-guided displacement scanning strategy [3] and by nested searching [7]. Although effective, these techniques are time consuming and/or only applicable to deal with small inter-image deformations; besides, they may require manual interactions as well [3], [8].

In this paper, a new correlation-based stereovision technique is proposed. The whole workflow is adapted to track features in sequential frames of one camera and register them to the equivalent frames of the stereo pair. The proposed technique assumes that the cameras are fixed and the objects are moving dynamically.

Feature displacements are modeled by separate shape functions for each feature subset. The parameters of the shape functions are determined by optimizing a correlation criterion via particle swarm optimization (PSO). Photogrammetric space intersection is applied to extract the three-dimensional state vector of each feature. Concisely, the salient points worked on are:

- accurate and careful lens and sensor calibration of the cameras,
- precise calibration of the stereo setup,
- avoiding the drawbacks of non-linear adjustments for digital image correlation by the automatic search algorithm of PSO,
- confining and accelerating the search flow by object-based constraints,
- reducing interpolation time,
- simultaneous 3D deformation measurement, and
- relative accuracy evaluation by means of check marks.

The paper structure is organized as follows. In the next section, the proposed methodology of this study is discussed in detail. The experimental aspects are presented thereafter. The results of the experiments and, finally, the conclusion are discussed in sections 3 and 4.

2. METHODOLOGICAL WORKFLOW

The main workflow of this study is illustrated in Fig.1. The following five subsections are dedicated to explaining the principal procedures.

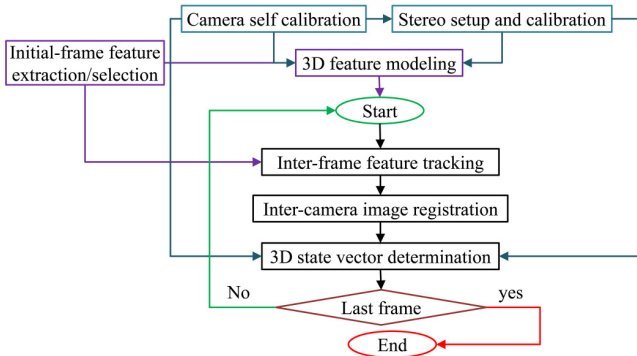


Fig.1. Methodological diagram of the correlation-based stereovision measurement system.

A. Camera calibration

Interior orientations are the terms applied to mathematically describe the parameters involved in modeling the geometry of light rays passing through the lens and hitting the image plane. The principal distance and the coordinates of the principal point¹ are the main interior orientation parameters, which should be measured when any camera is used for high-accuracy modeling. While a metric digital camera is characterized by stable, known and repeatable interior orientation parameters, those of non-metric cameras, as within this study, are unstable and undefined [8].

Such lenses suffer from aberrations, some of which can be minimized by adjusting the image acquisition and aperture parameters. In more professional camera systems, lens aberration correction functions are provided too. They are mostly capable of modifying lens issues, such as peripheral illumination (vignetting), chromatic aberration like coma, color blur, and astigmatism. Some of these aberrations may also be correctable by post image-processing techniques.

Although all the aberrations affect image quality, the aberrations known as radial and decentering distortions, which affect the geometry (location) of image elements [9], are the only ones considered in this work. Their impacts cannot be alleviated by aperture setting, and they need to be modeled accurately.

In-plane sensor distortions, which are caused by electronic deficiencies of sensor manufacturing, should also be considered as factors affecting the modeling accuracy; the most concerning in-plane distortion parameters are known as shear and scale of sensor elements.

The task of measuring interior orientation parameters and modeling lens and sensor distortions is called camera calibration. Calibration of the digital cameras, in this study,

¹ The principal distance is the perpendicular distance from the perspective center to the image plane and the principal point is where the optical axis, passing through the lens center, hits the focal plane.

is performed by the standard photogrammetric self-calibration method, by which calibration parameters are estimated through a bundle adjustment [8].

A stereo setup, for 3D photogrammetric measurements, urges the input of camera exterior orientation parameters in order to reconstruct the 3D information involved. As such, the platform calibration for determining the relative orientation parameters between two cameras is mandatory [6], [9]. These parameters include three translation and three rotation parameters defining the imaging coordinate system of one camera with regard to the other one. In this study, a true-scale test-field is applied for calibration purposes.

B. Feature tracking and image registration

Once the features are defined on the first frame, the task is to track them from the first to the next one. Briefly, the problem is to track each feature located at the known position (x_0^t, y_0^t) on the t^{th} frame, and to find its correspondence located at an unknown position (x_0^{t+1}, y_0^{t+1}) on the $t+1^{\text{th}}$ frame. Assuming a sub-window of $N \times N$ pixels, for the pixels (x_i^{t+1}, y_j^{t+1}) belonging to this window, a first-order displacement mapping function can be written as follows [3].

$$\begin{bmatrix} x_i^{t+1} \\ y_j^{t+1} \end{bmatrix} = \begin{bmatrix} x_i^t \\ y_j^t \end{bmatrix} + \begin{bmatrix} \alpha \\ \beta \end{bmatrix} + \begin{bmatrix} \alpha_x \cdot (x_i^t - x_0^t) \\ \beta_x \cdot (x_i^t - x_0^t) \end{bmatrix} + \begin{bmatrix} \alpha_y \cdot (y_j^t - y_0^t) \\ \beta_y \cdot (y_j^t - y_0^t) \end{bmatrix} \quad (1)$$

The matching criterion applied in this study is a correlation function called zero-normalized sum of squared difference (C_{ZNSSD}). This correlation function is highly recommended by the literature, as it is capable of compensating unexpected intensity changes [2], [10], [11].

Assuming that I^t is the intensity image of frame t and I^{t+1} is that of frame $t+1$, then, the correlation of two image windows can be formulated as:

$$C_{ZNSSD} = \frac{\sum_{i=1}^N \sum_{j=1}^N \left[\frac{I^t(x_i^t, y_j^t) - \bar{I}^t}{\sqrt{\sum_{i=1}^N \sum_{j=1}^N (I^t(x_i^t, y_j^t) - \bar{I}^t)^2}} \right]}{\frac{I^{t+1}(x_i^{t+1}, y_j^{t+1}) - \bar{I}^{t+1}}{\sqrt{\sum_{i=1}^N \sum_{j=1}^N (I^{t+1}(x_i^{t+1}, y_j^{t+1}) - \bar{I}^{t+1})^2}}} \quad (2)$$

where: $\bar{I} = 1/N^2 \times \sum_{i=1}^N \sum_{j=1}^N I(x_i, y_j)$.

Therefore, the tracking problem can be re-formatted to an optimization problem, where the objective function is (2), and the variables are six deformation parameters $(\alpha, \beta, \alpha_x, \beta_x, \alpha_y, \beta_y)$.

To solve this problem, standard particle swarm optimization is applied [12]. PSO is originally inspired by the concerted behavior of swarms of birds or insects. In standard PSO, a swarm of particles flying through D-

dimensional parameter space of solutions (here six-dimensional) are considered. The particles move to get to the best destination, which is the solution for the parameters and maximizes the objective function. PSO begins by generating a set of random particles to form the initial population. While flying, each particle adjusts its trajectory (velocity and position) towards its own best solution (the cognitive component) and the global best solution (the social component). The velocity and position of particle i in dimension j at iteration k are represented as $V_{i,j}^k$ and $P_{i,j}^k$; they get updated by the following equation.

$$\begin{aligned} P_{i,j}^{k+1} &= P_{i,j}^k + V_{i,j}^{k+1} \\ V_{i,j}^{k+1} &= w \times V_{i,j}^k + c_1 \times r_1 (pbest_{i,j} - P_{i,j}^k) + c_2 \times r_2 (gbest_j - P_{i,j}^k), \end{aligned} \quad (3)$$

In (3), w controls acceleration or changing rate of velocity, which is known as inertia weight; it decides how much the previous flight direction of a particle might influence its new direction. The larger w is, the more diversity will be achieved among solutions. In this study, w is set to 0.9, and is decreased linearly to 0.4 at the end [13]. Since the search space (variation of shape parameters from one pair of frames to another) is not large, setting inertia weight to a very high or a very low value can cause rapid acceleration or deceleration [14].

Accordingly, c_1 and c_2 are two weight factors, which determine the proportions of cognitive and social components correspondingly; and, r_1 and r_2 are random numbers uniformly distributed in the range of [0,1]. $pbest_{i,j}$ is the best solution of particle i in dimension j ; and $gbest_{i,j}$ is the best solution of all particles in dimension j (up to iteration k). Using c_1 and c_2 , one can decide how much a particle relies on its own direction and how much confidence it has in other individuals. As other PSO parameters, there have been various schemes in the literature to determine c_1 and c_2 . To guarantee the convergence of the swarm to an equilibrium state, the method of [15] is used here, which keeps a balance between the social component, cognitive component, and inertia weight [16]. By this method, value of c_1 is decreased and value of c_2 is increased linearly between 0.5 and 1; i.e., more exploration is applied initially, and more attraction to the best global solution is directed at the end [16].

The fitness or goodness of each particle i is determined by the correlation function (2). The update process is iteratively continued until the maximum number of iterations is reached or the maximum correlation is achieved. In this experiment, the maximum number of iterations is set to 50. However, the quality of a solution when reaching the maximum number of iterations can be tested by the fitness achieved. If the best global fitness had been relatively constant for the last generations, then the solution could not have been further improved. This can be statistically expressed as the standard deviation of the fitness values of $gbests$ from last generations.

Having been tracked to the next frame of the reference camera, the features should be registered to their corresponding ones on the target image by stereo registration. Assuming that the reference feature is located at

(x_0^{ref}, y_0^{ref}) on the reference image, then its corresponding coordinate on the target image is (x_0^{tar}, y_0^{tar}) . We can define a shape function between reference sub-window, centered at the feature, and the unknown target sub-window [17]. The same correlation function and PSO algorithm of inter-frame feature tracking is applied to register the stereo images by the shape function of (4).

$$\begin{bmatrix} x_i^{tar} \\ y_j^{tar} \end{bmatrix} = \begin{bmatrix} G_1 \\ G_4 \end{bmatrix} + \begin{bmatrix} G_2 & G_3 \\ G_5 & G_6 \end{bmatrix} \begin{bmatrix} x_i^{ref} \\ y_j^{ref} \end{bmatrix} \quad (4)$$

C. Gray value interpolation

Regarding (2), the gray values, $I(x_i, y_j)$, at sub-pixel locations are required to calculate the correlation function. The traditional method is to perform sup-pixel interpolation at each position, when necessary. However, this apparently straightforward approach is extremely time-consuming with high computational expense. Following the idea developed by [3], a pre-computed global look-up table of interpolation coefficients is formed for each sub-image to eliminate repetitive interpolation calculations at sub-pixel locations and to speed up the optimization process. Applying such look-up table does not affect the accuracy of interpolation, as it does not propose an approximate alternative. Instead, it avoids numerous passages of the original image as callee to an external interpolation function for every feature.

The interpolation function applied in this study is a bilinear one. For each pixel location (P, Q) four interpolation coefficients (A, B, C, D) are calculated by (5) to fill the look-up table. Given a sub-pixel location $(P'+p, Q'+q)$, where P' and Q' are the integer parts, and p and q are the fractional parts, the gray value is computed by searching for the coefficients A', B', C', D' corresponding to P', Q' at the look-up table as (6).

$$\begin{aligned} A &= I(P, Q); B = I(P, Q+1) - I(P, Q); C = I(P+1, Q) - I(P, Q) \\ D &= I(P+1, Q+1) + I(P, Q) - I(P+1, Q) - I(P, Q+1) \end{aligned} \quad (5)$$

$$I(P'+p, Q'+q) = A' + B' \times q + C' \times p + D' \times p \times q \quad (6)$$

D. 3D State vector measurement

When the features of an epoch are detected on the reference frame and co-registered to the target frame, their object-space coordinates can be computed from the collinearity equations [8]. If (x_n^{ref}, y_n^{ref}) and (x_n^{tar}, y_n^{tar}) are the coordinates of feature n on reference and target images, respectively, then the following four observation equations are solved by least squares adjustment to extract the 3D object-space coordinates of the feature, (X_n, Y_n, Z_n) :

$$\begin{aligned} X_n - T_x - (Z_n - T_z) \frac{U^{tar}}{W^{tar}} &= 0; X_n - Z_n \frac{U^{ref}}{W^{ref}} = 0 \\ Y_n - T_y - (Z_n - T_z) \frac{V^{tar}}{W^{tar}} &= 0; Y_n - Z_n \frac{V^{ref}}{W^{ref}} = 0 \end{aligned} \quad (7)$$

where,

$$\begin{bmatrix} U \\ V \\ W \end{bmatrix}^{ref} = \begin{bmatrix} x_n^{ref} + \Delta x_n^{ref} \\ y_n^{ref} + \Delta y_n^{ref} \\ -f^{ref} \end{bmatrix} \text{ and,} \quad (8)$$

$$\begin{bmatrix} U \\ V \\ W \end{bmatrix}^{tar} = R_1(\omega).R_2(\varphi)R_3(\kappa) \begin{bmatrix} x_n^{tar} - x_p^{tar} + \Delta x_n^{tar} \\ y_n^{tar} - y_p^{tar} + \Delta y_n^{tar} \\ -f^{tar} \end{bmatrix}.$$

In the above equations, $(\omega, \varphi, \kappa)$ are the rotation angles of the imaging coordinate system of the target camera relative to the reference imaging coordinate system, and (T_x, T_y, T_z) are the coordinates of the target camera perspective center relative to the reference camera. The parameters f, x_p and y_p are the interior orientation parameters of the cameras, which are accurately determined in the calibration process; R_1, R_2, R_3 are the fundamental rotation matrices, and $(\Delta x, \Delta y)$ are systematic errors due to lens and sensor distortions, which are calculated using camera calibration parameters by (9).

$$\begin{aligned} \Delta x &= (x - x_p)(K_1 r^2 + K_2 r^4 + K_3 r^6) + P_1(r^2 + 2(x - x_p)^2) \\ &+ 2P_2(x - x_p)(y - y_p) + A_1(x - x_p) + B_1(y - y_p) \\ \Delta y &= (y - y_p)(K_1 r^2 + K_2 r^4 + K_3 r^6) + P_2(r^2 + 2(y - y_p)^2) \\ &+ 2P_1(x - x_p)(y - y_p) \end{aligned} \quad (9)$$

The radial and decentering lens distortion coefficients are (K_1, K_2, K_3) and (P_1, P_2) , respectively. A_1 and B_1 are sensor distortion coefficients, and r is the radial distance from the principal point.

The other elements of the 3D state vector are the feature velocity and acceleration (\vec{V}_n, \vec{a}_n) , which are calculated as the first- and second-order derivatives of position over the frame rate (Δt) :

$$\vec{a}_n^t = \frac{\vec{X}_n^{t+1} - 2\vec{X}_n^t + \vec{X}_n^{t-1}}{\Delta t^2}, \quad \vec{V}_n^t = \frac{\vec{X}_n^{t+1} - \vec{X}_n^t + \vec{X}_n^{t-1}}{\Delta t} + \vec{V}_n^{t-1} \quad (10)$$

E. PSO confinement

Assuming a short frame interval and constant motion at this interval, the approximate object-space coordinates of feature n at epoch $t+1$ can be calculated by its position, velocity and acceleration at previous epochs using the following kinematic approximation.

$$\vec{X}_n^{t+1} = \vec{X}_n^t + \frac{\vec{a}_n^{t-1}}{2} \Delta t^2 + \vec{V}_n^{t-1} \Delta t \quad (11)$$

Using \vec{X}_n^{t+1} , the collinearity equations (7) are applied in inverse way to calculate the approximate value of feature position on frame $t+1$, (x_0^{t+1}, y_0^{t+1}) . Considering the frame rate, this approximation is accurate enough to set the initial values of (α, β) equal to $(x_0^{t+1} - x_0^t, y_0^{t+1} - y_0^t)$ and the affinity parameters to zero. The search range (limits for particle velocity on each dimension) is assigned accordingly as the

maximum and minimum of the values of each displacement model parameter from frame $t-10$ to frame t . In basic PSO, this is called velocity clamping [16].

3. EXPERIMENTS AND RESULTS

This study can be considered more as a preliminary proposal of a new methodology, which is put into a simple experiment herein. Two digital cameras are applied, which are both calibrated using the multi-resolution, multi-depth test-field of Fig.2. (left). The cameras are Canon camcorders with 3.28 megapixels resolution and 1/4.85" CMOS sensors [18]. The 32x zoom lenses of the cameras are fixed to wide angles, resulting in the exact focal lengths of 4.821 mm and 4.830 mm.

Once the cameras are fixed at their stereo locations, the external orientation parameters of both cameras can be calculated by taking videos from the non-moving board of calibration targets. These exterior orientation parameters can be used as they are for further calculations. However, as explained in section 2.D, measurements are more straightforward if the imaging coordinate system of the reference camera is set as the zero reference. Therefore, relative orientation is applied, where the horizontal base is set to its real value calculated from exterior orientation parameters, for keeping the real-world scale. The orientation parameters $(T_x, T_y, T_z, \omega, \varphi, \kappa)$ are 1430.401 mm, 196.708 mm, -552.034 mm, -2.217°, -43.443°, and 2.461°, respectively.

An experimental object is created by printing the pattern of rusty metal, plus evaluation marks, on paper and pasting it on a piece of wooden board (Fig.2. (right)). The pattern size is approximately 50x30 cm. The features are selected by the Harris corner detector from the first image and matched manually to the target image. The centers of the circular targets (1.5 cm diameter) are also precisely determined and added to the list of features to be tracked. In order to evaluate the accuracy of the matching process, the circular targets are used as check marks; i.e., they are both tracked along with other features and measured separately by a circular target detection algorithm as described by author's previous work [18].

The object board is moved and rotated in various directions in the view field of the cameras. The average distance of the object from the cameras is less than two meters. The video frame rate is 1/60 second; however, the algorithm is performed by rate of 1/30. The following paragraphs discuss the results obtained from this experiment.

Fig.3. illustrates the amount of the systematic error due to lens and sensor distortions, and offset of principal point, as in (10), for the reference camera. It can be noticed that these distortions are large enough to leave noticeable impacts on measurement accuracy, a comprehensive study of which is reviewed by [9]. For example, consider a feature located at pixel (1500, 800); then, the systematic error at two directions is (11.50, -4.47) pixels. This means that the straight ray from this object should have hit the sensor at position (1511.50, 795.53); however, this feature is seen at (1500, 800) because of an ensemble of lens and sensor

distortions. Assuming a distance of 2 meters from the camera parallel to the object-space coordinate system, the imaging scale is 0.0024. In this case, ignoring the systematic error would cause an average object measurement error of 12.17 mm; which is an important error in close-range applications.



Fig.2. The multi-resolution, multi-depth test-field for camera calibration test-field (left) and the object pattern designed from rusted metal texture and circular evaluation marks (right).

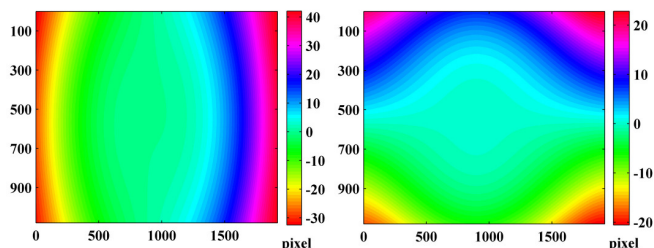


Fig.3. Lens and sensor distortions modeled at horizontal (left) and vertical directions (right).

The matching error is defined as the difference of tracked and registered check marks from their positions determined by the circle detection algorithm. The average error of check marks is plotted against the frame number (successively) for reference and target cameras, namely tracking and registration errors (Fig.4.). The root mean square error (RMSE) of tracking through 1270 frames (with 30 Hz rate) is 0.1550 and 0.1273 pixel in horizontal and vertical directions, respectively; and the RMSE of stereo image registration is 0.0948 and 0.1874 pixel in horizontal and vertical direction, respectively.

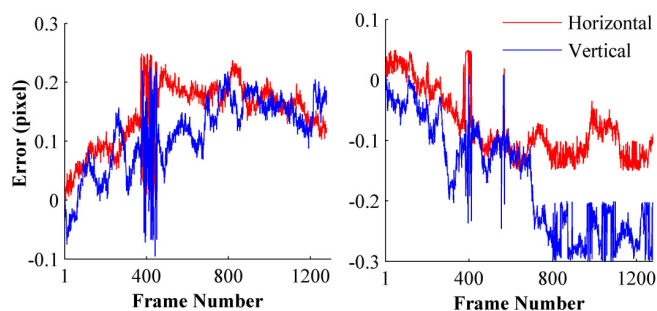


Fig.4. Average inter-frame feature tracking error (left) and stereo image registration error (right).

To assess the relative accuracy of 3D dynamic measurements, the 3D distances between independent pairs of evaluation marks are calculated from the results of the stereovision technique. Since the circles are originally plotted at pre-determined locations and are relatively fixed on the flat board, their true distances are known. Thus, the residuals remaining by subtracting the calculated distances from the pre-specified distances reveal the accuracy of displacement measurement in terms of magnitude. The average magnitude error of displacement measurement is represented in Fig.5. (left). The same method is applied to assess the relative accuracy of orientation. The 3D angles between check marks are calculated from their position vectors, and they are compared with the true, pre-defined angles. Fig.5. (right) illustrates the average orientation error of motion measurement versus the frame number. In summary, displacement measurement is performed in 3D by RMS magnitude error of 0.3568 millimeter and orientation error of 0.3298 degree.

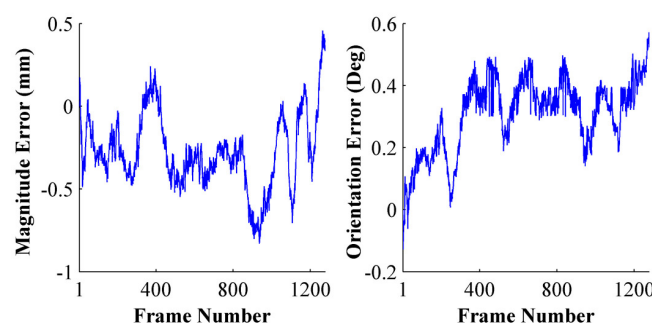


Fig.5. Deformation measurement error versus successive frame numbers. Magnitude error in millimeters (left) and orientation error in degrees (right).

There are several important factors that affect the tracking and registration accuracy, such as radiometric distortions and robustness of shape functions. Efficiency of shape functions can be remarked when the object status is changed significantly and quickly, during a very short period of the video. Under this condition, the first-order displacement mapping function is not efficient in modeling the real movement of the features. Besides, the assumption of constant acceleration between adjacent frames is not valid any more. Furthermore, the motion blur, caused by changes faster than video frame rate, affects the visibility of features. Therefore, tracking and registration would result in lower accuracy. This effect can be observed in Fig.4. and Fig.5., where measurement accuracy is changed considerably for several frames around frame 400. Fig.6. shows the status of the object in four different close frames (from left to right: frames 371, 381, 436, and 449). It can be observed that inter-frame tracking has lower accuracy during this period of video, since estimating the shape function is more difficult when the initial assumptions of the algorithm are not completely true. However, this error is not equally revealed in inter-camera registration, because it is a relative matching, and the check marks are imposed to similar distortions in both cameras' videos. Accordingly, the registration error affects the 3D measurements, especially

orientation accuracy. This can be explained by the fact that quick movements of the object are more rotational rather than translational. As a conclusion, this drawback of the algorithm should be considered in future investigations by applying more robust modeling functions and radiometric techniques of motion compensation.



Fig.6. Object status in four close frames.

4. CONCLUSIONS AND FUTURE WORK

In this paper, a new correlation-based stereovision technique is proposed to perform inter-frame feature tracking and stereo image registration, and to measure the 3D state vectors of features. The proposed algorithm is based on particle swarm optimization aided by object-based initialization. This technique eliminates the drawback of non-linear numerical optimization techniques that require very accurate initial approximations, since PSO is not trying to solve any non-linear functions mathematically, and its search space can be adaptively extended to ensure convergence. Furthermore, it eliminates the necessity of computing sub-pixel intensity gradients at each pixel, which reduces the processing time significantly.

Resulting in relative 3D measurement accuracy of 0.4 millimeters, the proposed methodology of this study can be considered as an effective method for monitoring very small-range motions of different structures. The size of the studied object in this experiment is several centimeters; however, depending on the spatial resolution and ground coverage of cameras, larger objects of several meters can be modeled as well. Moreover, this algorithm can be extended to perform stereo-registration between a reference camera and several target cameras. This would increase the robustness of measurements as the geometric configuration for photogrammetric intersection would be enhanced. Besides, the coverage area extended by several cameras increases the chance of modeling larger objects.

As mentioned before, this study is a preliminary proposal, which is still under development. Therefore, in the future, the system needs to be tested on more complex study objects involving more complicated deformations and displacement, and during a longer video period. Its performance should also be compared with other similar methods. It is also considered to improve the selection of PSO parameters using more sophisticated methods, as proposed by [19]. Currently, they are determined empirically and based on simple selection theories in this paper. As another point of concern, PSO can be replaced with other heuristic search algorithms and their performance can be compared.

The author is also interested in reducing the stereovision system to a monocular one as suggested by [20], where the images are recorded using a single camera and a series of mirrors playing the role of virtual cameras.

REFERENCES

- [1] Pan, B., Qian, K., Xie, H., Asundi, A. (2009). Two-dimensional digital image correlation for in-plane displacement and strain measurement: A review. *Measurement Science and Technology*, 20 (6), 062001.
- [2] Hu, Z., Xie, H., Lu, J., Hua, T., Zhu, J. (2010). Study of the performance of different subpixel image correlation methods in 3D digital image correlation. *Applied Optics*, 49 (21), 4044-4051.
- [3] Pan, B., Li, K. (2011). A fast digital image correlation method for deformation measurement. *Optics and Lasers in Engineering*, 49 (7), 841-847.
- [4] Cheng, P., Sutton, M.A., Student, H.W.S.P.D., McNeill, S.R. (2002). Full-field speckle pattern image correlation with B-spline deformation function. *Experimental Mechanics*, 42 (3), 344-352.
- [5] Vendroux, G., Knauss, W.G. (1998). Submicron deformation field measurements: Part 2. Improved digital image correlation. *Experimental Mechanics*, 38 (2), 86-92.
- [6] Garcia, D., Orteu, J.J., Penazzi, L. (2002). A combined temporal tracking and stereo-correlation technique for accurate measurement of 3D displacements: Application to sheet metal forming. *Journal of Materials Processing Technology*, 125, 736-742.
- [7] Zhang, Z.F., Kang, Y.L., Wang, H.W., Qin, Q.H., Qiu, Y., Li, X.Q. (2006). A novel coarse-fine search scheme for digital image correlation method. *Measurement*, 39 (8), 710-718.
- [8] Luhmann, T., Robson, S., Kyle, S.A., Harley, I.A. (2006). *Close Range Photogrammetry: Principles, Techniques and Applications*. John Wiley & Sons.
- [9] Lava, P., Van Paepegem, W., Coppieters, S., De Baere, I., Wang, Y., Debruyne, D. (2013). Impact of lens distortions on strain measurements obtained with 2D digital image correlation. *Optics and Lasers in Engineering*, 51, 5576-584.
- [10] Pan, B., Wu, D., Xia, Y. (2012). An active imaging digital image correlation method for deformation measurement insensitive to ambient light. *Optics & Laser Technology*, 44 (1), 204-209.
- [11] Chen, F., Chen, X., Xie, X., Feng, X., Yang, L. (2013). Full-field 3D measurement using multi-camera digital image correlation system. *Optics and Lasers in Engineering*, 51, 1044-1052.
- [12] Kennedy, J., Eberhart, R. (1995). Particle swarm optimization. In *IEEE International Conference on Neural Networks*, November 1995. IEEE, Vol. 4, 1942-1948.
- [13] Shi, Y., Eberhart, R.C. (1999). Empirical study of particle swarm optimization. In *CEC 99 : Congress on Evolutionary Computation*, July 1999. IEEE, Vol. 3, 1945-1950.
- [14] Khosla, A., Kumar, S., Aggarwal, K.K., Singh, J. (2006). Particle swarm for fuzzy models identification. In Nedjah, N., Mourelle, L.M. (eds.) *Swarm Intelligent Systems*. Studies in Computational Intelligence. Springer, 149-173.

- [15] Ratnaweera, A., Halgamuge, S., Watson, H. (2002). Particle swarm optimization with self-adaptive acceleration coefficients. In *First International Conference on Fuzzy Systems and Knowledge Discovery: Computational Intelligence for the E-Age*, November 2002. Singapore: Nanyang Technological University, 264–268.
- [16] Engelbrecht, A.P. (2007). *Computational Intelligence: An Introduction* (2nd ed.). John Wiley & Sons.
- [17] Gruen, A. (1985). Adaptive least squares correlation: A powerful image matching technique. *South African Journal of Photogrammetry, Remote Sensing and Cartography*, 14 (3), 175-187.
- [18] Shahbazi, M. (2013). 2.5D feature tracking and 3D motion modeling. *International Journal of Computer Applications*, 64 (5), 43-50.
- [19] Zhao, J.Q., Zeng, P., Lei, L.P., Ma, Y. (2012). Initial guess by improved population-based intelligent algorithms for large inter-frame deformation measurement using digital image correlation. *Optics and Lasers in Engineering*, 50 (3), 473-490.
- [20] Pankow, M., Justusson, B., Waas, A.M. (2010). Three-dimensional digital image correlation technique using single high-speed camera for measuring large out-of-plane displacements at high framing rates. *Applied Optics*, 49 (17), 3418-3427.

Received June 30, 2013.
Accepted November 18, 2013.